The computation of flow and heat transfer through square-ended U-bends, using low-Reynolds-number models

Konstantinos-Stephen P. Nikas
Department of Mechanical Engineering, Laboratory of Aerodynamics, National Technical University of Athens (NTUA), Athens, Greece

Hector Iacovides
Department of Mechanical, Aerospace and Manufacturing Engineering, UMIST, Manchester, UK

Received February 2003
Revised May 2003
Accepted June 2003

Keywords *Flow measurement, Heat transfer, Turbulent flow, Modelling*

Abstract *This study is concerned with the computation of turbulent flow and heat transfer in U-bends of strong curvature. Following the earlier studies within the authors' group on flows through round-ended U-bends, here attention is turned to flows through square-ended U-bends. Flows at two Reynolds numbers have been computed, one at 100,000 and the other at 36,000. In the heat transfer analysis, the Prandtl number was either 0.72 (air) or, in a further departure from our earlier studies, 5.9 (water). The turbulence modelling approaches examined, include a two-layer and a low-Re k-ε model, a two-layer and a low-Re version of the basic differential stress model (DSM) and a more recently developed, realisable version of the differential stress model that is free of wall-parameters. For the low-Re effective viscosity model (EVM) and DSMs, an alternative, recently proposed length-scale correction term, independent of wall distance has also been tested. Even the simplest model employed – two-layer EVM – reproduces the mean flow development with reasonable accuracy, suggesting that the mean flow development is mainly influenced by mean pressure rather than the turbulence field. The heat transfer parameters, on the other hand, show that only the low-Re DSMs produce reliable Nusselt number predictions for both Prandtl numbers examined.*

Nomenclature

c_1, c_2, c_1^w, c_2^w, c_1, c_1', c_2, c_2'	= turbulence modelling constants	P	= pressure
		P_{ij}	= production rate of the Reynolds stress
c_t, c_μ	= coefficients	Pr	= Prandtl number
f_1, f_2, f_μ, f_H, f_J	= damping functions	T, t	= mean, fluctuating temperature
f_{w1}, f_{w2}, f_{w3}, f_{w1}', f_{Rt}, f_{Rt}, f_{Rt}', f_A	= coefficients in the Craft/NYap model	U_i, $i = 1, 2, 3$	= contravariant velocity components
k	= turbulent kinetic energy	$\overline{u_i u_j}$	= Reynolds stress tensor
NYap	= new, differential, Yap correction term	$\overline{u_i t}$	= turbulent heat flux
		x_i, $i = 1, 2, 3$	= Cartesian coordinates

International Journal of Numerical Methods for Heat & Fluid Flow
Vol. 14 No. 3, 2004
pp. 305-324

0961-5539
DOI 10.1108/09615530410517977

Greek symbols

δ_{ij}	= Kronecker delta	ν, ν_t	= kinematic, kinematic eddy viscosity
ε ε_{ij}, ε'_{ij}, ε''_{ij}, ε'''_{ij}	= dissipation rate of k	ρ	= density
μ, μ_t	= molecular, eddy viscosity	σ_k, σ_ε, σ_t	= turbulent Prandtl numbers

Introduction

Flow and heat transfer through tight square-ended U-bends, shown in Figure 1, provides an idealised representation of the flow and thermal processes present in internal cooling passages of gas-turbine blades. In modern gas-turbines, relatively cold air extracted from the compressor, is used through internal cooling passages to cool the turbine discs, the nozzle guide vanes and the turbine blades to maintain the operating temperature of the blades at safe levels. The flow development and the heat transfer characteristics inside these cooling passages are complex and highly three-dimensional influenced by the presence of sharp U-bends, artificial rib-roughness and the rotation of the blades. For these reasons, flow and heat transfer through such passages have been the subject of a number of numerical and experimental investigations such as those of Ekkad and Han (1995), Metzger and Sahm (1986) and Rigby and Ameri (1996).

In two-dimensional flows through curved channels, the most critical problem is the modelling of effects of streamline curvature on the turbulence field. The effects of the streamline curvature on turbulence are caused by the centrifugal force. They are represented in the turbulence kinetic energy, stress transport and scale equations by terms involving interaction of different stress and rate of strain components. Early attempts in predicting the behaviour of such flows showed that conventional effective viscosity models (EVM) have all failed to reproduce these curvature effects. As shown by Iacovides and Li (1993) and Nemouchi (1988), to reproduce the measured mean flow development the use of second-moment closures becomes necessary.

In three-dimensional flows through curved ducts of moderate curvature, the main flow feature is the curvature-induced secondary motion. This is driven by the imbalance between the radial (cross-duct) pressure gradient and the centrifugal force. At the near-wall regions, due to the low axial velocity,

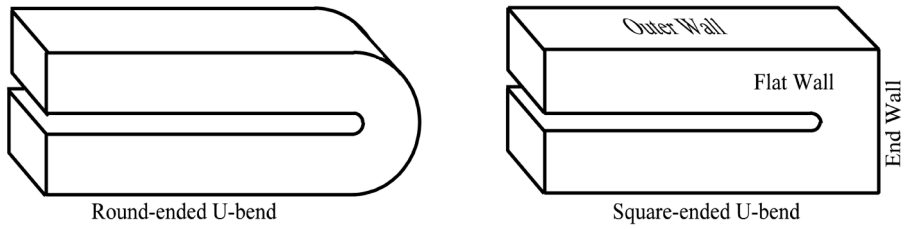

Figure 1.
Flow geometry

the centrifugal force is weak and the radial pressure gradient force drives the fluid towards the outer side of the curved duct. In the duct core, where the axial velocity is high, the centrifugal force is the dominant one and drives the fluid towards the outer side of the curved duct. The curvature-induced secondary motion can thus be reproduced even in computations using EVMs. As the secondary motion is strongest within the near-wall regions, where the imbalance between the centrifugal and radial pressure forces is greatest, one would expect that only turbulence models that resolve the near-wall motion would be able to reproduce this flow feature correctly. This has been shown to be the case by the work of Choi *et al.* (1989), who instead of using the high-Re turbulence models with the wall-function approximation, adopted a two-layer approach. This allows the mean flow equations to be integrated up to the wall, using simple models of near-wall turbulence. Choi *et al.* (1989) also showed that replacement of high-Re k-ε in the duct core with an algebraic second-moment closure resulted in further improvements in the predicted flow field. This suggests that the effects of turbulence anisotropy, while less critical than in two-dimensional flows through curved passages, are certainly not negligible. Iacovides *et al.* (1996a, b, c) subsequently showed that the introduction of a realisable, wall-parameter-free, second-moment closure for the core region, within a two-layer approach, produced marked improvements in the predicted thermal development.

For U-ducts of strong curvature the streamwise pressure gradients, present at the bend entry and exit, become strong enough to produce flow separation along the inner wall of the duct. This dominates the flow development over the second half of a 180° bend and in the region immediately after the bend exit. Bo *et al.* (1995a, b) and Iacovides *et al.* (1996a) presented computations of turbulent flow and heat transfer through a round-ended, square-cross-sectioned U-bend of a strong curvature ($R_c/D = 0.65$). The former study demonstrated that in order to obtain numerically accurate solutions, bounded high-order schemes had to be employed for the discretisation of the convection of the turbulent variables (k and ε) as well as of the mean flow variables. The latter study showed that the starting point of flow separation over the inner wall is more reliably predicted by models in which the anisotropy of turbulence in the near-wall sub-layers is also considered. Even with low-Re second-moment closures, however, flow separation along the inner wall was predicted to start later than what was found in the measurements.

The question therefore arises as to whether the conclusions reached from the above numerical studies of round-ended U-bends are also applicable to square-ended U-bends. As can be seen in Figure 1, square-ended U-bends introduce two additional complications in comparison to round-ended ones. On the one hand, there are two sharp 90° corners along the outer wall of the U-bend which are likely to cause flow separation, and on the other hand the continuous change in cross-sectional area around the bend gives rise to additional

streamwise pressure gradients. Moreover, as flow visualization tests carried out by Iacovides *et al.* (1999) show, over the second half of the square ended U-bend, the turbulent flow also becomes unsteady. Large-scale instabilities were observed, which however die down soon after the bend exit. Further evidence on flow instabilities are provided in the recent numerical study of Chung *et al.* (2003), concerning laminar flow through a U-bend of similar geometry. The main motivation for that investigation was the internal cooling of electronic circuits. Chung *et al.* (2003) found that above a critical Reynolds number, laminar flow becomes unsteady as it goes through a square-ended U-bend. In contrast to the experimental findings of Iacovides *et al.* (1999) on turbulent flows, by Chung *et al.* (2003) the numerical study of laminar flows showed that the large-scale instabilities dominated the flow development in the region downstream of the bend. The recent emergence of local flow and thermal data for square-ended U-bends from Ekkad and Han (1995) and Iacovides *et al.* (1999), provided the validation data necessary to answer this question and led to the present numerical study. What distinguishes this study from those carried out earlier in the field of U-bend flows, is that here, for the first time, we focus on square-ended U-bends. A further departure from our earlier studies is that the heat transfer computations are at present carried out for water as well as for air. The primary objective here is to assess the effectiveness of low-Re models similar to those we previously applied to flow computations through round-ended U-bends, while a further objective has been to introduce and assess the effectiveness of a recently developed realisable second-moment closure (Craft, 1998).

Theoretical model

The flow computations have been obtained through the solution of the Reynolds-averaged flow equations, presented here in Cartesian tensor notation.

Continuity:

$$\frac{\partial}{\partial x_i}(\rho U_i) = 0 \tag{1}$$

Momentum:

$$\frac{\partial}{\partial x_j}(\rho U_j U_i) = -\frac{\partial P}{\partial x_i} + \frac{\partial}{\partial x_j}\left[\mu\left(\frac{\partial U_i}{\partial x_j} + \frac{\partial U_j}{\partial x_i}\right) - \rho\overline{u_i u_j}\right] \tag{2}$$

Energy:

$$\frac{\partial}{\partial x_j}(\rho T) = \frac{\partial}{\partial x_j}\left[\frac{\mu}{\mathrm{Pr}}\frac{\partial T}{\partial x_j} - \rho\overline{u_i t}\right] \tag{3}$$

Turbulence modelling

The turbulence models tested are as follows.

(1) A two-layer EVM.

(2) The Launder-Sharma low-Re EVM.

(3) A two-layer basic differential stress model (DSM).

(4) A basic low-Re DSM.

(5) The Craft realisable low-Re DSM.

The first two of the above models are widely used and well known. Their equations are thus not included in this section. The equations for the less well known, two layer and also the low-Re basic DSM, which have been employed in all computations are included. The Craft low-Re DSM is a more recently developed and more complex closure. The terms representing the redistribution of turbulence have been derived by imposing realisability conditions, which also satisfy the two-component limit of turbulence and are of cubic order in terms of the strain rates. Near-wall damping is provided through both turbulence Reynolds number and stress invariants. Inhomogeneity parameters based on the gradients of the turbulent length scale are also introduced to represent the wall effects on the anisotropy of turbulence and also to provide the correct wall-limiting values for the dissipation rates of the Reynolds stresses. The conventional wall-reflection terms that use the wall distance and the wall-normal direction are thus not needed. This model has been successfully used to compute a number of test cases, which include channel flows, free-surface flows and stagnation flows. Inevitably, it leads to a more complex set of transport equations for the turbulent stresses and the dissipation rate. Owing to space limitations the equations for this model are not presented here. Interested readers can refer to Craft (1998).

Effective viscosity models

In both EVM versions, the Reynolds stresses and the turbulent heat fluxes are obtained from the effective viscosity and effective diffusivity approximations, respectively.

$$\rho\overline{u_i u_j} = \frac{2}{3}k\delta_{ij} - \mu_t\left(\frac{\partial U_i}{\partial x_j} + \frac{\partial U_j}{\partial x_i}\right) \tag{4}$$

$$\overline{u_i t} = -\frac{\mu_t}{\sigma_T}\frac{\partial T}{\partial x_i} \tag{5}$$

This is a widely used approach, popular for its numerical robustness, but which produces an isotropic turbulent viscosity field. In most flows the contribution of the normal strain rates to the levels of the normal stresses in equation (4) is fairly minor. Consequently, the turbulence energy is distributed

equally in all directions $\left(\bar{u_1^2} \simeq \bar{u_2^2} \simeq \bar{u_3^2} \simeq (2/3)k\right)$. Turbulence is however anisotropic and in many types of flows, such as flows with streamline curvature, the mean flow development is sensitive to the anisotropy of turbulence.

Two-layer k-ε/one-equation model. As the above name suggests, in the fully-turbulent region the standard high-Re version of the k-ε model is used, while in the near-wall regions a low-Re version of a one-equation model of k-transport is employed. This approach allows the resolution of the mean flow across the viscous wall sub-layer without the need to use an excessively fine near-wall grid.

In high-Re k-ε model, the turbulent viscosity that appears in equations (4) and (5) is obtained from the turbulent kinetic energy, k, and its dissipation rate.

$$\mu_t = \rho c_\mu k^2/\varepsilon \tag{6}$$

The "standard" high-Reynolds-number versions of the transport equations for k and ε are used to determine the distributions, of these two variables.

In the near-wall regions the distribution of k is still obtained through the numerical solution of the high-Re form of the transport equation, but the dissipation rate, ε, and the turbulent viscosity μ_t, are obtained from algebraic expressions, proposed by Wolfshtein (1969), that rely on prescribed length scales based on the wall distance.

The parameter $y^* \equiv Yk^{1/2}/\nu$ is the dimensionless wall distance, used to provide the wall damping of turbulence.

Low-Re k-ε model (Launder and Sharma, 1974). This is an extension of the high-Re k-ε that can reproduce the wall damping of turbulence and hence can be used across the viscous sub-layer. Instead of solving a transport equation for the real dissipation rate ε, we now solve for the "isotropic rate" $\tilde{\varepsilon}$. This is related to ε through the expression

$$\varepsilon = \tilde{\varepsilon} + 2\nu\left(\frac{\partial\sqrt{k}}{\partial x_j}\right)^2.$$

In the fully turbulent core, $\varepsilon = \tilde{\varepsilon}$. At the wall, $\tilde{\varepsilon} = 0$, while ε remains finite. A number of damping functions are included, in which the damping parameter R_t, is the local Reynolds number of turbulence, defined as $R_t \equiv k^2/(\nu\tilde{\varepsilon})$.

Low-Re DSM

The DSM closures employed here are rather simple and empirically derived extensions to the basic DSM, which relies on the linear redistribution terms and use the wall-reflection terms. They have evolved from the low-Re algebraic stress closures (ASM) proposed by Iacovides and Launder (1992) and initially applied to flow and heat transfer through U-bends of mild curvature. They were subsequently extended by Iacovides and Toumpanakis (1993) to low-Re

DSM closures and were initially applied to the computation of turbulent flows through rotating cavities (Iacovides *et al.*, 1996a, b, c), where they produced satisfactory predictions. These low-Re DSM closures have also been applied more recently by Iacovides (1999) and Iacovides and Raisee (2001) to the computation of flow and heat transfer through ribbed passages, where again their introduction improved the thermal predictions. The low-Re terms, constants and damping functions have been determined with reference to fully-developed pipe flow and have not been changed in any of the subsequent applications.

Instead of the effective viscosity approximation, equation (4), the turbulent stresses are obtained through the solution of separate transport equations, represented by equation (7).

As in the k and ε transport equations, the transport of the turbulent stresses due to turbulent mixing is modelled through the effective diffusivity concept. The term ε_{ij} denotes the dissipation rate of the turbulent stresses which, as shown in equation (9), is assumed to be isotropic when the flow is fully turbulent and proportional to the ratio $\overline{u_i u_j}/k$ at the wall. The function f_ε is zero when the flow is fully turbulent and one at the wall.

A set of equations for the basic low-Re DSM is as follows.

$$\frac{\partial}{\partial x_j}\left(\rho U_k \overline{u_i u_j}\right) = \frac{\partial}{\partial x_k}\left[\left(\mu + \frac{\mu_t}{\sigma_k}\right)\frac{\partial \overline{u_i u_j}}{\partial x_k}\right] + P_{ij} - \rho\varepsilon_{ij} + \varphi_{ij} - \left[H_{ij} - \frac{1}{3}H_{kk}\delta_{ij}\right] + J_{ij} \tag{7}$$

$$P_{ij} = \left(\overline{u_i u_k}\frac{\partial U_j}{\partial x_k} + \overline{u_j u_k}\frac{\partial U_i}{\partial x_k}\right) \tag{8}$$

$$\varepsilon_{ij} = \frac{2}{3}(1 - f_\varepsilon)\varepsilon\delta_{ij} + f_\varepsilon\frac{\overline{u_i u_k}}{k}\varepsilon \tag{9}$$

$$\varphi_{ij} = -c_1\frac{\varepsilon}{k}\left(\overline{u_i u_j} - \frac{2}{3}k\delta_{ij}\right) - c_2\left(P_{ij} - \frac{2}{3}P_k\delta_{ij}\right) + f_w\left(\varphi^w_{ij,1} + \varphi^w_{ij,2}\right) \tag{10}$$

$$\varphi^w_{ij,1} = -c^w_1\frac{\varepsilon}{k}\left(\overline{u_k u_m}n_k n_m\delta_{ij} - \frac{3}{2}\overline{u_k u_i}n_k n_j - \frac{3}{2}\overline{u_k u_j}n_k n_i\right)\left\{\frac{k^{1.5}}{\varepsilon c_l x_n}\right\} \tag{11}$$

$$\varphi^w_{ij,2} = -c^w_2\frac{\varepsilon}{k}\left(\varphi_{km2}n_k n_m\delta_{ij} - \frac{3}{2}\varphi_{ik2}n_k n_j - \frac{3}{2}\varphi_{jk2}n_k n_i\right)\left\{\frac{k^{1.5}}{\varepsilon c_l x_n}\right\} \tag{12}$$

where

$$\varphi_{ij2} = -c_2\left(P_{ij} - \frac{2}{3}P_k\delta_{ij}\right) \tag{13}$$

$$H_{ij} = f_H\frac{\nu}{k}\left(\overline{u_iu_l}\frac{\partial\sqrt{k}}{\partial x_l}\frac{\partial\sqrt{k}}{\partial x_j} + \overline{u_ju_l}\frac{\partial\sqrt{k}}{\partial x_l}\frac{\partial\sqrt{k}}{\partial x_i}\right) \tag{14}$$

$$J_{ij} = f_Jk\left(\frac{\partial U_i}{\partial x_j} + \frac{\partial U_j}{\partial x_i}\right)J_{ij} \tag{15}$$

$$\overline{u_it} = -\rho c_T\frac{k}{\varepsilon}\overline{u_iu_j}\frac{\partial T}{\partial x_j} \tag{16}$$

The term φ_{ij}, given in equation (10), represents the redistribution of turbulent energy among the different components of the Reynolds stress tensor due to fluctuations in the pressure and strain fields. Terms φ_{ij1}^{w} and φ_{ij2}^{w}, given in equations (11)-(13), are the conventional wall reflection terms, proposed by Gibson and Launder (1978), to model the "wall-echo" part of the pressure strain correlation. They have been devised for the fully turbulent region of a flow over a plane wall and make use of the wall distance x_n and the unit vector normal to the wall n.

Within the viscous sub-layer the wall reflection terms are damped through the function f_w. Their task within the viscous sub-layer is then performed by $(H_{ij} - H_{kk}\delta_{ij}/3)$, where H_{ij} is given by equation (14). The contribution of this term is more extensively discussed by Bo *et al.* (1995a, b). It represents a relatively simple way of achieving approximately the correct distribution of the Reynolds stresses across the viscosity-affected sub-layer. The term J_{ij}, given in equation (15), increases the sensitivity of the model to the effects of low mean flow Reynolds number. The turbulent heat fluxes are obtained through the generalised gradient diffusion hypothesis, given by equation (16).

Simplified (two-layer) DSM closure

In the *fully turbulent* region, ε is obtained from the same equation used in the high-Re k-ε model. In the *near-wall* region, ε is obtained from the wall distance, as in the Wolfshtein (1969) model $\varepsilon = k^{3/2}/l_\varepsilon$, but with:

$$l_\varepsilon = 2.55Y[1 - \exp(-0.263y^*)] \tag{17}$$

The damping functions that appear in equations (9)-(15) depend on the dimensionless wall distance y^* and have the following expressions:

$$f_\varepsilon = \exp(-y^*/3) \tag{18}$$

$$f_w = [1 - \exp(-0.12y^*)][1 + \exp(-0.03y^*)] \tag{19}$$

$$f_J = 0.06\exp(-y^*/3) \tag{20}$$

$$f_H = (10.2 + 7.5y^*)\exp(-y^*/20) \tag{21}$$

Low-Re DSM closure

The dissipation rate equation is the same as the corresponding equation of the low-Re k-ε model. The damping functions that appear in equations (9)-(15) depend on the turbulent Reynolds number, R_t, and have the following expressions:

$$f_\varepsilon = \exp(-R_t/8) \tag{22}$$

$$f_w = [1 - \exp(-R_t/20)][1 - \exp(-R_t/100)] \tag{23}$$

$$f_J = 0.06\exp(-R_t/8) \tag{24}$$

$$f_H = (10 + 2.6R_t)\exp(-R_t/20) \tag{25}$$

Also f_μ, which still appears in the stress and ε transport equations, is obtained from:

$$f_\mu = \exp[-4/(1 + 0.01R_t)^2] \tag{26}$$

As mentioned earlier, the damping functions shown in equations (18)-(26) have been devised with reference to fully-developed pipe flows and not specifically for the ribbed passage flows presented in this study.

Length scale correction terms

It is well known that in separated flows, the Launder-Sharma version of the ε equation returns excessively high levels of near-wall turbulence. To address this problem Yap (1987) proposed the addition of a correction term, YC, to the right-hand side of the ε equation, based on the wall distance, Y.

$$\mathrm{YC} = \max\left[0.83\frac{\tilde{\varepsilon}^2}{k}\left(\frac{k^{1.5}/\tilde{\varepsilon}}{2.55Y} - 1\right)\left(\frac{k^{1.5}/\tilde{\varepsilon}}{2.55Y}\right), 0\right] \tag{27}$$

In a recent proposal by Hanjaliç (1996), the wall distance in the above term is eliminated by using the gradient of the length scale normal to the wall surface. Here, these ideas are further developed by:

(1) introducing the resultant of the length scale gradient vector, and

(2) also considering the effects of wall damping across the sub-layer.

From Woolfshtein (1969):

$$l_\varepsilon = 2.55Y[1 - \exp(-0.263y^*)] \tag{28}$$

Differentiating l_ε and then replacing y^* by R_t, as proposed by Yap (1987), produces the following expression for the gradient of the equilibrium length scale, (dl_ε/dY) :

$$(dl_\varepsilon/dY) = c_l[1 - \exp(-B_\varepsilon R_t)] + B_\varepsilon c_l R_t \exp(-B_\varepsilon R_t) \quad (29)$$

with $c_l = 2.55$ and $B_\varepsilon = 0.1069$

From the resultant gradient, Dl, of turbulent length scale, $l = k^{3/2}/\varepsilon$, a correction factor F is defined according to:

$$Dl = \{(dl/dx_j)(dl/dx_j)\}^{1/2} \quad (30)$$

and

$$F = [Dl - (dl_\varepsilon/dY)]/c_l \quad (31)$$

A new version of the Yap term can then be developed, NYC of the form:

$$\mathrm{NYC} = \max[c_Y F(F+1)^2 \rho \varepsilon^2/k, 0] \quad (32)$$

Iacovides and Raisee (1999) initially suggested that c_Y, should have the value of 0.83, as in the original Yap term, for both low-Re k-ε and low-Re DSMs. Craft (1998) also adopted this term for his realisable DSM, for the low-Re DSM c_Y is set to 0.5, while for the low-Re k-ε it is left as 0.83.

The modelling of other constants that appear in the preceding equations have the values given in Table I.

Numerical aspects

A three-dimensional non-orthogonal finite volume solver, STREAM, has been employed, developed at UMIST, which employs the Cartesian velocity decomposition. A collocated grid is used. The SIMPLE algorithm is employed for the calculation of the pressure field, with the Rhie and Chow (1983) flux modification. In the case of DSMs, the apparent viscosity concept is used to prevent numerical oscillations that arise from the explicit presence of the Reynolds stress gradients in the momentum equations. For the convective discretisation of all transport equations, a bounded form of the quadratic upstream interpolation scheme (QUICK), proposed by Iacovides (1999), was used.

Table I. Turbulence modelling constants

c_μ	σ_k	c_1	c_2	c_1^w	c_2^w	c_T	σ_T
0.09	1	1.8	0.6	0.5	0.3	0.32	0.9

Presentation and discussion of results

As shown in Figure 1, the flow geometry is that of a square-ended U-bend of square cross-section in the straight tangents, with a ratio of 0.15 between the radius of the inner wall and the duct diameter. The flow domain started three duct diameters before the bend entry and extended to nine diameters after its exit. Two grids have been employed, the first consisting of 31×58 grid nodes over the half cross-section and 104 planes in the streamwise direction and the second consisting of 45×86 grid nodes over the half cross-section and 104 streamwise planes. As shown in Figure 2(a), the mean and turbulent flow fields produced by the two grids are practically identical. Figure 2(b) shows that the differences in the local Nusselt number distributions produced by the two grids are only minor. It thus appears that the grids used in combination with the

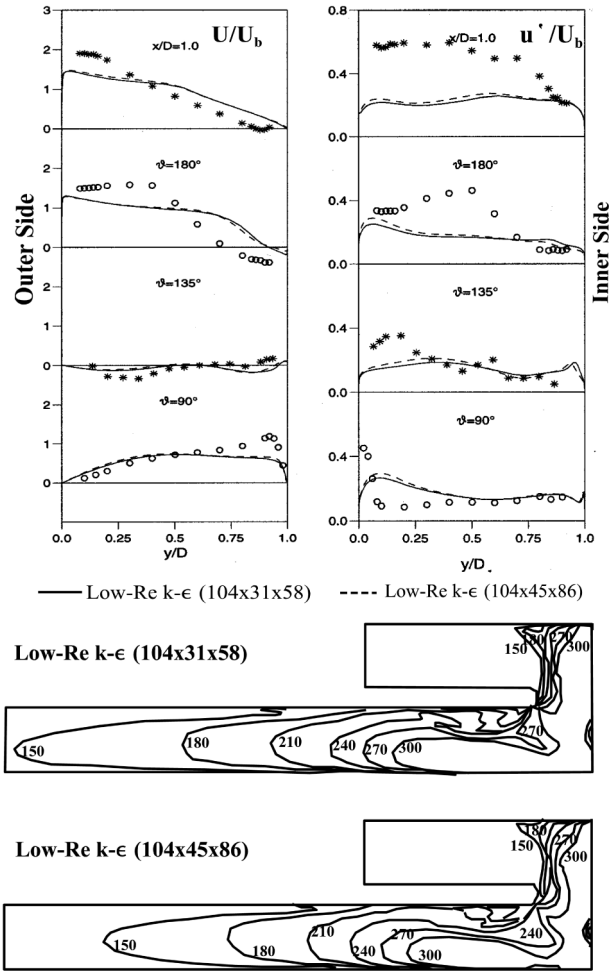

Figure 2.
Comparison of mean flow field and local Nusselt number distributions for grid dependency reasons

bounded QUICK scheme ensure that numerical errors do not contaminate the predictions. Computations have been carried out at two flow Reynolds numbers, namely 36,000 and 100,000. Heat transfer computations have been obtained with constant wall heat flux boundary conditions, at Prandtl number values of 0.72 and 5.9. At $Pr = 0.72$, all duct walls were heated, while at $Pr = 5.9$, only the two flat walls were heated, to be consistent with available heat transfer data. Fully developed duct flow hydrodynamic and thermal entry conditions have been prescribed and generated through preliminary computations.

Comparisons of the mean velocity field along the duct symmetry plane, shown in Figure 3, indicate that all the turbulence models return a largely similar mean flow development. The differences between the k-ε and DSM predictions are smaller than those identified in our earlier studies of round-ended U-bends (Iacovides *et al.*, 1996a, b, c). This suggests that mean flow development is mainly influenced by the strong streamwise pressure gradients caused by the continuous change in cross-sectional area around the bend. The main flow features present in the measurements are reproduced, but all models return a narrower than measured separation bubble along the inner wall. The realisable DSM produces a slower recovery after the bend exit than the other models. More detailed mean flow comparisons are provided by the profiles of the streamwise velocity in Figure 4. The failure of all models to predict the correct size of the separation bubble at the bend exit is clearly evident, while the differences between the predictions of the realisable DSM and those of the other models in the first two downstream diameters are also noticeable. Comparisons further downstream, not shown here, suggest that the slower downstream recovery produced by the realisable DSM are in contrast to the measured behaviour.

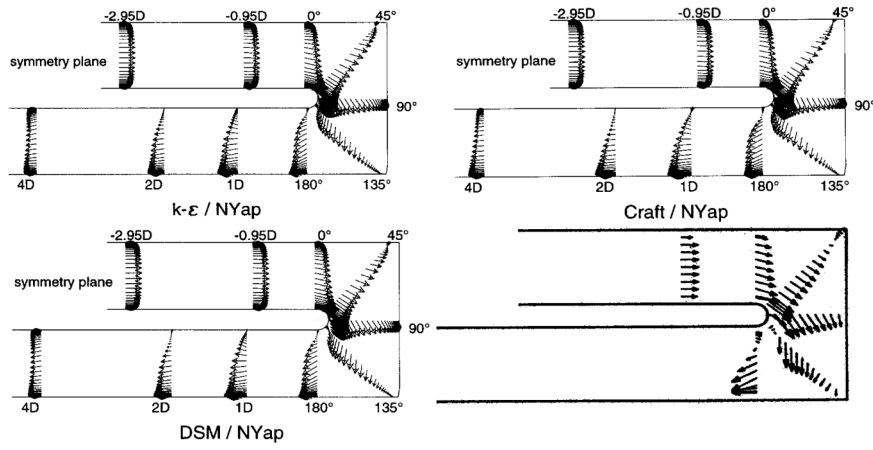

Figure 3.
Comparison between computed and measured mean flow fields along the duct symmetry plane

Source: Iacovides *et al*. (1999)

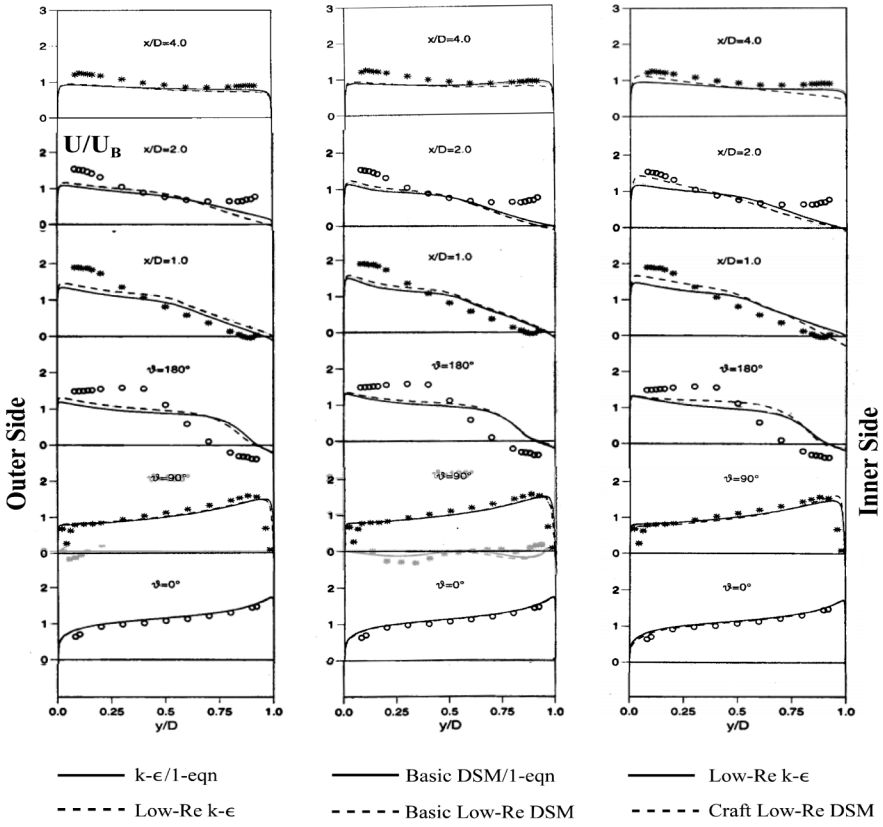

Source: Iacovides *et al*. (1999)

Figure 4.
Comparison between computed and measured profiles of the axial velocity along duct symmetry plane ○○○○

Figure 5 compares the computed development of the secondary motion within the bend with that inferred from the available measurements. The data show that the classical two-vortex structure prevails throughout the turn, with the vortices becoming significantly more intense at the 90° plane, where the cross-sectional area is narrowest and then weakening somewhat by the 135° plane. To some extent, at the 135° plane, the effects of the increase in cross-sectional area on the secondary motion are offset by the presence of a sizeable separation bubble along the inner wall. The measurements also show that the flow within the bend is significantly non-symmetric. As noted earlier, flow visualisation tests carried out by the experimental investigators (Iacovides *et al.*, 1999), showed that this is caused by flow instabilities within the bend which die down after the bend exit. The present computations assume both a plane of symmetry and steady conditions and consequently cannot reproduce this phenomenon. At the 45 and 90° planes, all computations reproduce the two-vortex structure. At the 135° plane, because the predicted separation

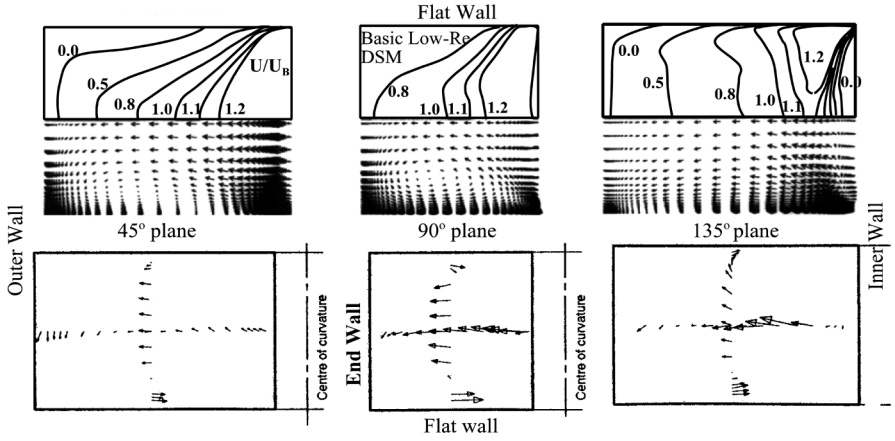

Figure 5.
Comparison between predicted and measured cross-duct flow fields within the turn

Source: Iacovides *et al*. (1999)

bubble is smaller than the one observed in the experiment, the computed secondary motion is noticeably weaker. Moreover, in contrast to the measurements, the computations show that almost over the entire cross-section, the cross-duct motion is predominantly in the outward direction. This disappearance, from the predictions, of the two-vortex structure, appears to be caused by the fact that the thickness of the boundary layer along the flat walls is suppressed, resulting almost in two-dimensional variation of axial velocity from the inner to the outer wall. The Craft DSM closure, not included here, returns a weaker secondary motion than the basic low-Re DSM, which is consistent with the general slower flow development returned by the Craft model. The other models, also not shown here, produce mean flow predictions similar to those of the basic low-Re DSM.

The profiles of the streamwise turbulence intensity, shown in Figure 6, reveal that all models severely under-predict intensity levels at and immediately after the bend exit. Within the turn, the EVMs return higher intensities than the basic DSM closures, while after the turn the situation is reversed. The realisable Craft model produces intensity distributions similar to those of the basic DSM, but somewhat of lower levels. One possible explanation may be that the measured intensities also include the effects of the large-scale instabilities observed within the turn. Indeed, as noted in the "Introduction", the recent numerical work of Chung *et al.* (2003) on laminar flows provides further support for this. This suggests that in future, time-dependent computations should be attempted, using either unsteady Reynolds-averaged Navier-Stokes (RANS) or detached eddy simulation.

Heat transfer computations on the other hand, such as the ones shown in Figure 7, for a Prandtl number of 0.72, show greater sensitivity to the

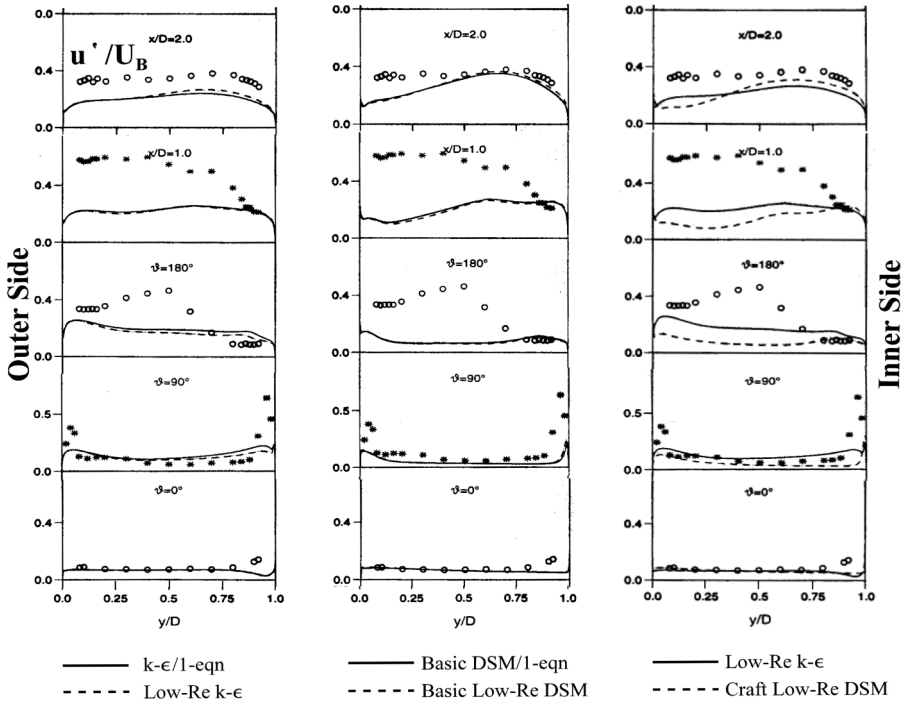

Source: Iacovides *et al*. (1999)

Figure 6.
Comparison between computed and measured profiles of the axial component of turbulence intensity along symmetry plane. ○○○○

turbulence models employed. The side-averaged Nusselt number measurements in Figure 6 were obtained at a Reynolds number of 60,000, while the predicted values were for a Re value of 100,000 and were then scaled for a value of 60,000 through the Dittus-Böelter formula. All the models under-predict Nu levels within and after the bend. Not surprisingly, the two-layer models, especially the two-layer k-ε, return the lowest Nu levels. There is relatively little difference between the low-Re predictions produced by the two alternative versions of the Yap term, especially for the basic DSM, with the predictions of the basic DSM marginally closer to the data than those of the low-Re k-ε. The realisable (Craft) DSM while predicting reasonable Nu levels after the bend, within the bend it severely under-predicts the Nusselt number.

Comparisons between the measured contours of the local Nusselt number and those predicted by the basic DSM with the differential version of the Yap term are shown in Figure 8. The measurements show that the Nusselt number starts to increase as the fluid enters the turn and a local peak is reached over the first half of the turn, near the end wall. This must be caused by impingement of the fluid entering the turn on the end wall. Over the second half of the turn, the

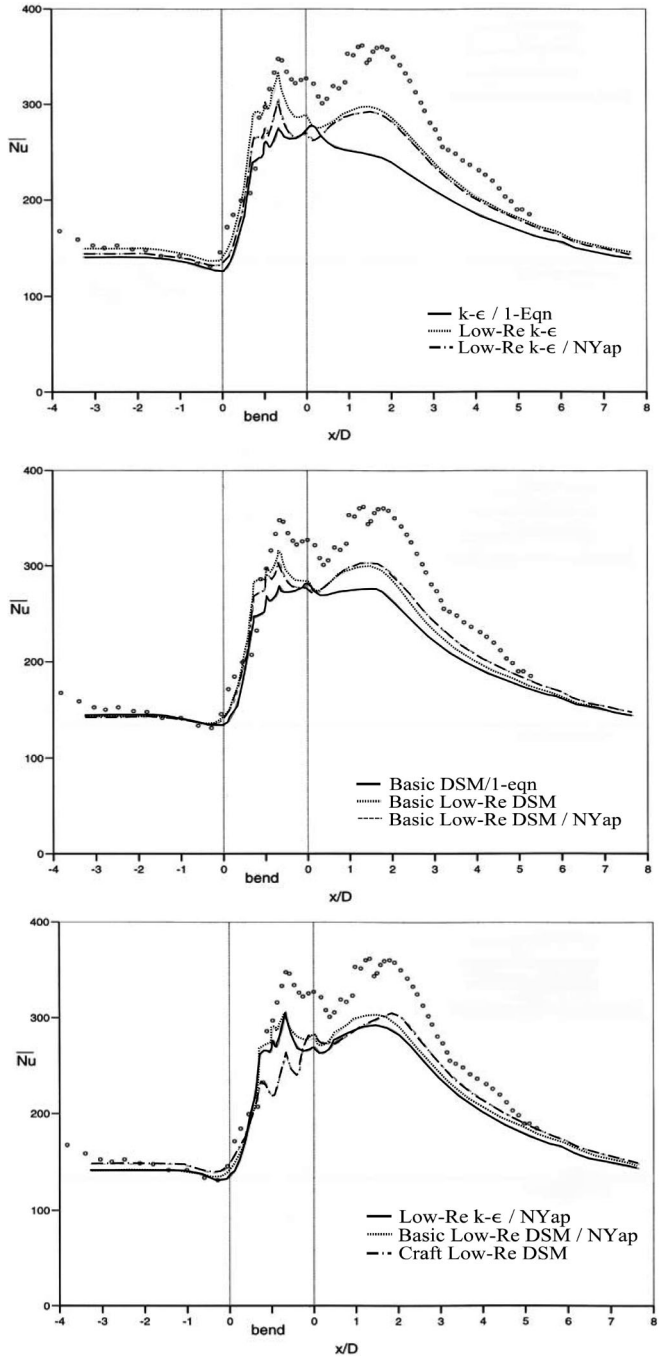

Figure 7.
Comparisons of the axial variation of the side averaged Nusselt number along the flat wall. Re = 60,000 and Pr = 0.72

Source: Ekkad and Han (1995)

Nusselt number reaches a local minimum at the corner between the end and the outer walls. At the bend exit, the measured Nusselt number is high along the outer side, where the flow accelerates, and low along the inner side where there is a separation bubble. Further downstream, the high Nusselt number levels along the outer side spread over the entire flat wall, while after the first three downstream diameters the measured Nusselt number starts to fall. Most of these features are returned by this model and the overall Nusselt number levels are well predicted. Perhaps the greatest predictive deficiency of the model is its failure to return the low Nusselt number levels at the downstream corner of the bend, a feature consistent with the erroneous prediction of the outward motion at the 135° plane, identified in Figure 5. Further discrepancies between the thermal predictions and the corresponding measurements include a slower rise in Nusselt number at the bend entry, larger regions of high Nusselt number in the bend and downstream and also a larger region of low Nusselt number along the inner side at the bend exit.

When the Prandtl number increases, the thickness of the conduction sub-layer, the thermal equivalent of the viscous sub-layer, are reduced, making the coefficient of wall heat flux more sensitive to variations in near-wall turbulence and consequently its prediction more sensitive to the modelling of near-wall turbulence. The latter is clearly evident in the comparisons of Figure 9 that shows the measured and computed variation of the side-averaged Nusselt number for $Pr = 5.9$. The under-prediction of the upstream levels suggests that the experimental entry conditions were not thermally fully-developed. Within and downstream of the turn, in contrast to the comparisons at the lower Prandtl number, the two-layer models, especially the EVMs, return a reasonable variation, though in the middle of the turn the Nusselt number is over-predicted. The low-Re EVMs over-predict Nusselt number levels at the middle of the turn and also show a severe dip at the bend exit which is not present in the measurements. Both these predictive deficiencies are less severe in the basic low-Re DSM closures, with the prediction of the DSM closure that employs the differential form of the Yap term being notably closer to the measured distribution.

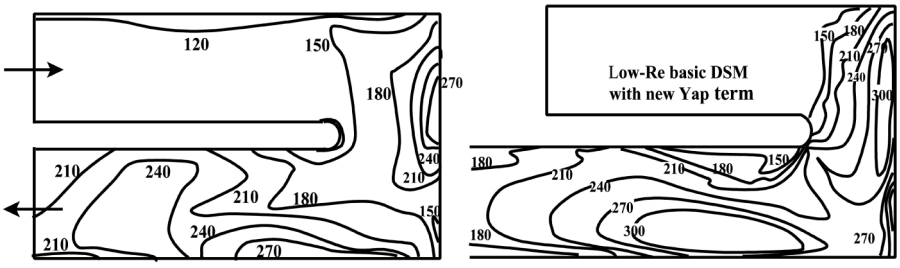

Source: Ekkad and Han (1995)

Figure 8.
Comparisons of local Nusselt number along the flat wall. $Re = 60{,}000$ and $Pr = 0.72$

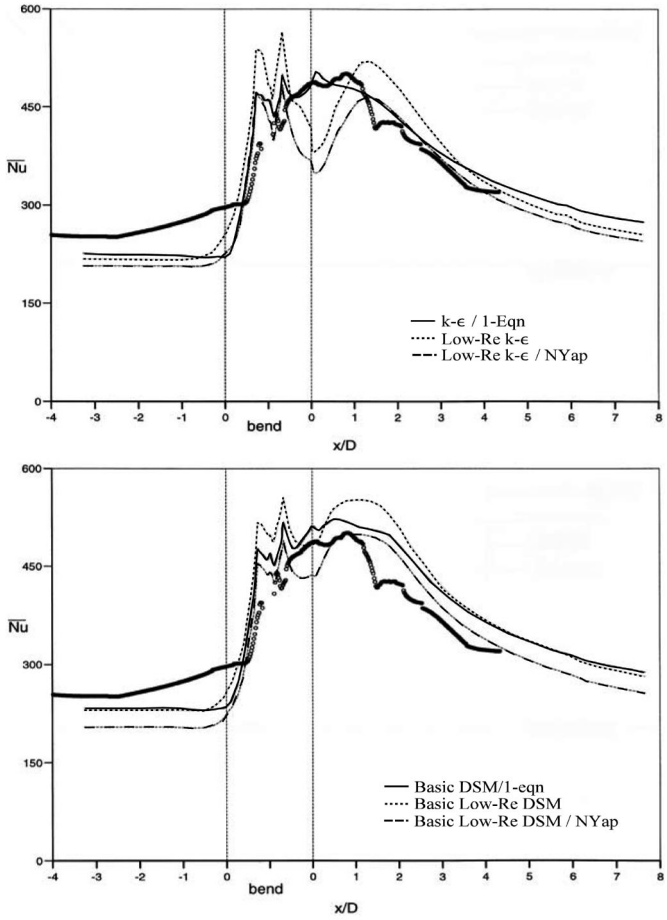

Figure 9.
Comparisons of the axial variation of the side averaged Nusselt number along the flat wall. Re = 36,000 and Pr = 5.9

Source: Iacovides *et al*. (1999)

Conclusions

The overall picture that emerges from these comparisons suggests that even the simplest model employed, two-layer EVM, reproduces the mean flow development with reasonable accuracy, suggesting that the mean flow development is mainly influenced by the pressure gradients, rather than the turbulence field. When commenting on the under-prediction of turbulence levels within the bend, the flow instabilities and indeed the lack of flow symmetry reported by the experimentalists within the bend needs to be borne in mind. The distribution of the local Nusselt number is better predicted for air (Pr = 0.72) than for water (Pr = 5.9). The predictions of Nusselt number are found to be sensitive to the modelling of both near-wall turbulence and turbulence anisotropy. Using the variation in side-averaged Nusselt number as

a guide, for air as the working fluid (Pr = 0.72) the low-Re models are superior to the two-layer models, though the Craft realisable DSM does not result in any additional improvements in comparison to the basic low-Re DSM. With water as the working fluid (Pr = 5.9), the average Nu predictions of the two-layer models move closer to the measurements, while among the low-Re models only the DSMs, especially with the differential Yap term, return reliable predictions of the average Nusselt number. It thus appears that only low-Re DSM models produce reliable Nusselt number predictions for a range of Prandtl numbers examined. For improvements in heat transfer predictions at higher Prandtl numbers the present comparisons suggest that the modelling of the turbulence decay across the viscous sub-layer needs to be further refined.

References

Bo, T., Iacovides, H. and Launder, B.E. (1995a), "Convective discretization schemes for the turbulence transport equations in flow predictions through sharp U-bends", *Int. J. Numer. Meth. Heat Fluid Flow*, Vol. 5, pp. 33-48.

Bo, T., Iacovides, H. and Launder, B.E. (1995b), "Developing buoyancy-modified turbulent flow in ducts rotating in orthogonal mode", *ASME Journal of Turbomachinery*, Vol. 117, pp. 474-84.

Choi, Y-D., Iacovides, H. and Launder, B.E. (1989), "Numerical computation of turbulent flow in a square-sectioned 180-deg bend", *ASME J. Fluids Eng.*, Vol. 111, pp. 59-68.

Chung, Y.M., Tucker, P.G. and Roychowdhury, D. (2003), "Unsteady laminar flow and convective heat transfer in a sharp 180° bend", *Int. J. Heat Fluid Flow*, Vol. 24, pp. 67-76.

Craft, T.J. (1998), "Prediction of heat transfer in turbulent stagnation flow with a new second-moment closure", *Proc. 2nd Int. Conf. Turbulent Heat Transfer*, Manchester, UK, Vol. 2, pp. 4.25-5.

Ekkad, S.V. and Han, J.C. (1995), "Local heat transfer distributions near a sharp 180° turn of a two-pass smooth square channel using a transient liquid crystal image technique", *Journal of Flow Visualization and Image Processing*, Vol. 2, pp. 285-97.

Gibson, M.M. and Launder, B.E. (1978), "Ground effects on pressure fluctuations in atmospheric boundary layers", *Journal of Fluid Mechanics*, Vol. 85, p. 391.

Hanjaliç, K. (1996), "Some resolved and unresolved issues in modelling non-equilibrium and unsteady tubulent flows", *Proc. 3rd Int. Symp. Engineering Turbulence Modelling and Measurements*, Crete, Greece.

Iacovides, H. (1999), "The computation of turbulent flow through stationary and rotating U-bends of with rib-roughened surfaces", *Int. J. Numer. Meth. Fluids*, Vol. 29, pp. 865-76.

Iacovides, H. and Launder, B.E. (1992), "The computation of convective heat transfer in a 180° pipe bend", *ICHMT, Int. Symp. Heat Trans. in Turbomachinery*, Athens, Greece.

Iacovides, H. and Li, H.-Y. (1993), "Near-wall turbulence modeling of developing flow through curved ducts and channels", *Proc. 5th Int. Symp. Refined Flow Modeling and Turbulence Measurements*, Paris, France.

Iacovides, H. and Raisee, M. (1999), "Recent progress in the computational flow and heat transfer in internal cooling passages of turbine blades", *Int. J. Heat Fluid Flow*, Vol. 20, pp. 320-8.

Iacovides, H. and Raisee, M. (2001), "Computation of flow and heat transfer in two-dimensional rib-roughened passages, using low-Reynolds number turbulence models", *Int. J. Numer. Meth. Heat Fluid Flow*, Vol. 11, pp. 138-55.

Iacovides, H. and Toumpanakis, P. (1993), "Turbulence modelling of flow in axisymmetric rotor-stator systems", *Proc. IAHR, 5th Int. Symp. Refined Flow Modelling and Turbulence Measurements*, Paris.

Iacovides, H., Launder, B.E. and Li, H-Y. (1996a), "The computation of flow development through stationary and rotating U-ducts of strong curvature", *Int. J. Heat Fluid Flow*, Vol. 17, pp. 22-33.

Iacovides, H., Launder, B.E. and Li, H-Y. (1996b), "Application of a reflection-free DSM to turbulent flow and heat transfer in a square-sectioned U-bend", *Int. J. Expt. Thermal Fluid Science*, Vol. 13, pp. 419-29.

Iacovides, H., Nikas, K.-S. and Te Braak, M.A.F. (1996c), "Turbulent flow computation in rotating cavities using low-Reynolds number models", Paper No. ASME-96-GT-159, Int. Gas-Turb and Aero Congress, Birmingham, UK.

Iacovides, H., Jackson, D.C., Kelemenis, G., Launder, B.E. and Yuan, Y-M. (1999), "Experiments on local heat transfer in a rotating square-ended U-bend", *Int. J. Heat Fluid Flow*, Vol. 20, pp. 302-10.

Launder, B.E. and Sharma, B.I. (1974), "Application of the energy-dissipation model of turbulence to the calculation of flow near a spinning disc", *Letrs Heat Mass Trans.*, Vol. 1, pp. 131-8.

Metzger, D.E. and Sahm, M.K. (1986), "Heat transfer around sharp 180° turns in smooth rectangular channels", *ASME J. Heat transfer*, Vol. 108, pp. 500-6.

Nemouchi, I.Z. (1986), "Computation of turbulent thin shear flows associated with flow around multi-element aerofoils", PhD thesis, Department of Mechanical Engineering, Faculty of Technology, University of Manchester.

Rhie, C.M. and Chow, W.L. (1983), "Numerical study of the turbulent flow past an airfoil with trailing edge separation", *AIAA Journal*, Vol. 21 No. 11, pp. 1525-32.

Rigby, D.L. and Ameri, A.A. (1996), "Internal passage heat transfer prediction using multi block grids and k-ε turbulence model", ASME Paper, 96-GT-188.

Wolfshtein, M. (1969), "The velocity and temperature distribution in one-dimensional flow with turbulence augmentation and pressure gradient", *Int. J. Heat Mass Transfer*, Vol. 12, p. 301.

Yap, C.R. (1987), "Turbulent heat and momentum transfer in recirculation and impinging flows", PhD thesis, Mechanical Engineering Department, UMIST.